International Journal of Engineering

Journal Homepage: www.ije.ir

Improving Super-resolution Techniques via Employing Blurriness Information of the Image

S. J. Seyyedyazdi, H. Hassanpour*

Faculty of Computer Engineering and IT, Shahrood University of Technology, Shahrood, Iran

PAPER INFO

Paper history:
Received 05 October 2017
Received in revised form 01 November 2017
Accepted 30 November 2017

Keywords:
Super-resolution
Blur Kernel
Blur Kernel Estimation
Neural Network

ABSTRACT

Super-resolution (SR) is a technique that produces a high resolution (HR) image via employing a number of low resolution (LR) images from the same scene. One of the degradations that attenuates performance of the SR is the blurriness of the input LR images. In many previous works in the SR, the blurriness of the LR images is assumed to be due to the integral effect of the image sensor of the acquisition device. However, in practice there are some other factors that blur the LR images, such as diffraction, motion of the object and/or acquisition device, atmospheric blurring and defocus blurring. To apply the super-resolution process accurately, the degradation model applied to HR image leading to LR ones needs to be known. In this paper, we aim to use the LR images blurriness to find the blurring kernel applied on the HR image. Hence, we setup a simulation experiment in which the blurring kernel is limited to be one of the predetermined kernels. In the experiment, the blurriness of the LR images is supposed to be unknown, and is estimated using a blur kernel estimation method. Then, the estimated blur kernels of the LR images are fed to an artificial neural network (ANN) to determine the blur kernels associated with the HR image. Experiment results show the use of determined blur kernels improves the quality of output HR image.

doi: *10.5829/ije.2018.31.02b.07*

1. INTRODUCTION

Super-resolution (SR) technique is a process to generate a high resolution (HR) image using one or more low resolution (LR) images from the same scene. Since in many applications a high resolution image is more useful than the low resolution one, SR has many applications, for example in surveillance systems, remote sensing, and medical imaging.

The acquisition process that is performed by the acquisition device, applies some degradations to the exposed scene and produces output LR image. These degradations include warping, blurring, down-sampling and adding noise (Figure 1). In many SR researches, the blurring phenomenon that applied to LR images is assumed to be due to the imaging sensor of the acquisition device [1]. But in practice, there are other sources of blurriness such as the diffraction of light, motion of the object and/or acquisition device that leads to motion blur, turbulence of the atmosphere between objects of the scene and the acquisition device that leads to atmospheric blurring, and placing the objects out of the focus area of the lens that leads to defocus blurring.

Using lexicographical notation, the SR problem is defined as follows. Let x be a $PN \times 1$ vector that represents the desired HR image, y be a $N \times 1$ vector that represents the LR image, and the relation between x and y is as following

$$y = D(P) \times x \quad (1)$$

where $D(P)$ is the down-sampling operation matrix and P is the decimation factor equivalent to the factor of increasing the resolution. In (1) for simplicity, the blurring effect and noise that usually occur in practice are ignored. They come to play soon. Hereafter for simplicity $D(P)$ is shown as D.

According to (1), to make x from y, the lost information by down-sampling operation is required to be restored in some manner. Apparently, this is impossible in practice.

*Corresponding Author's Email: h.hassanpour@shahroodut.ac.ir (H. Hassanpour)

Please cite this article as: S. J. Seyyedyazdi, H. Hassanpour, Improving Super-resolution Techniques via Employing Blurriness Information of the Image, International Journal of Engineering (IJE), IJE TRANSACTIONS B: Applications Vol. 31, No. 2, (February 2018) 241-249

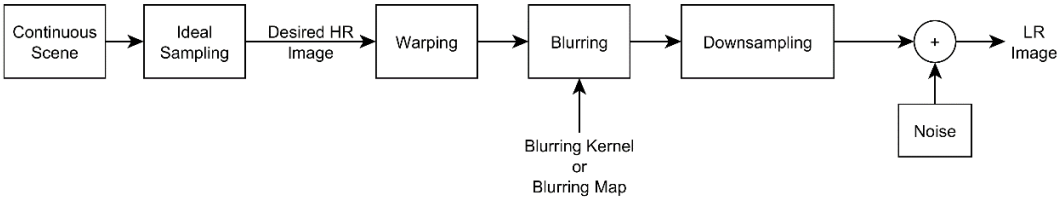

Figure 1. Block diagram of the observation or degradation model

To cope with this problem, SR uses multiple LR images. The LR images are taken from a scene in such a way that they be similar but not identical, which is performed by a little moving and/or rotating the imaging device. The effect of this movement/rotation is that the corresponding objects in LR images have some displacement (sub-pixel displacement) with respect to each other. These sub-pixel displacements are the corner stone of the SR.

Let there are L low resolution images of the scene. The kth LR image, y_k, is related to HR image x according to (2):

$$y_k = D \times H(h) \times W_k(s_k) \times x + n_k \quad (2)$$

where h is point spread function (PSF) or blurring kernel, $H(h)$ is the blurring operation matrix, s_k is warping parameter, $W_k(s_k)$ is warping operation matrix and n_k is noise. Hereafter the set of the LR images is shown as $\{y_k\}$.

Based on Equation (2) which is known as *observation* or *degradation model*, the original HR image x is warped, blurred and down-sampled respectively and finally is polluted with noise to make y_k. This process is depicted in Figure 1.

In SR problem, the LR images y_k are the inputs of the problem; D is constructed by knowing the increasing factor of resolution (i.e. P), and the warping parameters s_k and HR image x are assumed to be unknown. Often in literature, the blurring kernel h is assumed to be due to integrating effect of imaging sensor and is estimated as either average or Gaussian blurring kernel [2, 3]. This assumption is only fair if any other types of blurring have not engaged in acquisition process. If it is not the case, the blurriness of the LR images must be determined using detail information of acquisition process. But in practice, such information is rarely available. Hence there are two choices: providing blur kernel experimentally, or estimating it using blur kernel estimation methods. Investigating the later choice is the aim in this paper.

Organization of the paper is as following. Section 2 reviews the related works. In Section 3 the proposed method is presented. Section 4 shows experimental results and finally Section 5 concludes the paper.

2. LITERATURE REVIEW

Tsai and Huang published the first research on the super-resolution in 1984 [4]. Their method works in the frequency domain and uses the shifting property of the Fourier transform. SR has a big constraint in the frequency domain: the warping model that can be applied on the LR images is limited to be global translation. Hence, other common warping model such as rotation is not supported by the method. Due to the frequency domain limitation, other techniques often applied in special domain.

As mentioned in the Introduction Section, in many SR researches the blurriness of the LR images is assumed to be due to sensor integration effect. But there are a few studies that investigate blurriness in a wider perspective.

Tipping and Bishop used a parametric model for PSF [5]. Then, they estimate the parameter of the PSF as well as registration parameters using marginalization in a Bayesian framework. Nguyen et al. simplified the problem by using parametric point spread function [6]. They used generalized cross-validation to estimate both the PSF and regularization parameters. Aly and Dubois present a method to find an observation model that can produce the LR images from desired HR image [7]. Their algorithm cast the problem into an optimization framework using a power spectral density (PSD) model. Sroubek et al. did not assume any prior information about the shape of degradation blurs [8]. They built a regularized energy function and minimize it with respect to the original image and blurs. Laghrib et al. assumed another observation model in which the order of warping and blurring is different from (2) [9]. Hence they first reconstruct blurred HR image (Hx) and then deblur it to reconstruct HR image.

Farsiu et al. emphasize the need for research to provide a super-resolution method along with a general blur kernel estimation [2]. Following this, in this paper

we setup a simulation in which the blurring kernel is assumed to be one of the pre-specified blurring kernel. Then, by estimating blurring kernel of the LR images and knowing the *class* of blurring kernel of the HR image, we train an artificial neural network to identify the HR blurring kernel given an estimation of LR image blurring kernel. The blurring kernel is then used in the SR process.

3. EMPLOYING BLURRINESS INFORMATION IN SR

In this section the proposed method is presented. According to the observation model in (2), to reconstruct the desired HR image x, one must know the blurriness that applied to it. But, in practice such knowledge is not available and only the degraded LR images $\{y_k\}$ are accessible. To cope this problem, in this study we assume that there are a specific type of blurring kernels that may be applied on x in degradation process. The idea is to determine the type of blurring kernel for HR image x using known LR images $\{y_k\}$.

Based on the observation model (2), it is obvious that the nonlinearity property of the down sampling operator D makes the blurriness of the warped HR image $W_k x$ different from the blurriness of the LR images y_k. Hence, in this paper an artificial neural network (ANN) is used to predict the type of blurring kernel for HR image using the blurring kernel of the LR image.

To determine the blurring kernel, we setup a learning procedure. First, six blurring kernels of different types and sizes are chosen; specifically, average, Gaussian and disk blurring kernels each of which in sizes 5 and 11. We name the type/class of them as 1 to 6. Specifications of the blurring kernels are summarized in Table 1.

To train the ANN, first a dataset of LR/HR images using the six blurring kernels according to the observation model (2) was created. The same random warping parameters were applied to all images and the increasing factor in resolution was set to two ($P = 2$). Then, the blurriness of the created LR images was estimated using the blur kernel estimation algorithm presented in [10]. Finally, the estimated kernels and the class of the corresponding predetermined blur kernels were used as training data to train the ANN. The block diagram of the training system is shown in Figure 2.

The neural network that is used has one hidden layer with sixty neurons. We used Rectifier Linear Unit (ReLU) activation function for each neuron as it is a promising one in recent neural network literature (e.g. [11]) as well as it performs better than the traditional Sigmoid activation function in our study. The estimated 11×11 LR kernel is fed as a 121×1 vector to the ANN. The output of the ANN is a 6×1 vector corresponding to six blurring kernel classes.

To generate the training dataset, about 700 images from the imageNet Dataset [12] were selected. We tried to choose images that have no or little blurring. Some of the images are shown in Figure 3. The trained ANN, was then used to determine the HR blurring kernel. Then, the determined blurring kernel is fed to SR algorithm according to the block diagram in Figure 4.

4. EXPERIMENTS AND RESULTS

To evaluate our proposed system, the procedure is applied to sixty test HR images. Some of the test images are shown in Figure 5.

TABLE 1. Specification of the predetermined blurring kernels

Blur Type	size	parameter	Class number
Average	5×5	-	1
Average	11×11	-	2
Gaussian	5×5	3	3
Gaussian	11×11	5	4
Disk	5×5	-	5
Disk	11×11	-	6

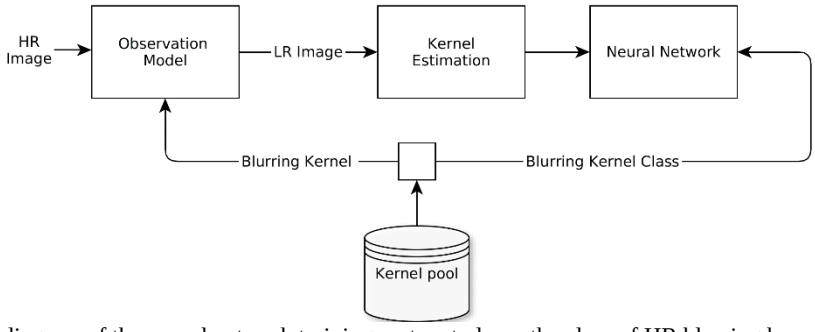

Figure 2. Block diagram of the neural network training system to learn the class of HR blurring kernel given LR ones

Figure 3. Some of the images used in the training dataset of neural network.

Specifically, ten LR images from each HR image were created according to the observation model, using the predetermined blurring kernel and same randomly warping parameter and the resolution increasing factor of 2.

The blur kernel class of each LR image is predicted by the neural network. It is obvious that various LR images captured from the same scene using the same device with same setting may not have different blurring kernel. Hence, for each pair of (a, b) where a is *LR image set*, and b is *predetermined blur kernel*, the predicted HR blur kernel is determined by voting between corresponding predicted LR's blur kernels.

The confusion matrix of predicted blur kernel classes before and after voting are shown in Tables 2 and 3, respectively.

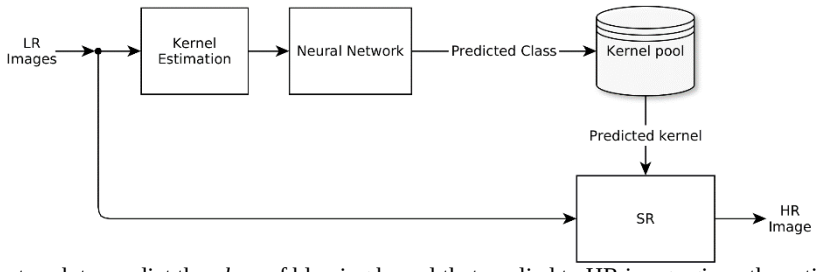

Figure 4. Using neural network to predict the *class* of blurring kernel that applied to HR image given the estimated blurring kernel of the LR images

TABLE 2. Confusion matrix before voting

		Actual class					
		1	2	3	4	5	6
Predicted class	1	90.83	0	20.17	0	1.5	0
	2	0.17	98.17	0.17	6	0.33	1.67
	3	8	0	78.17	0	9	0
	4	0.5	1.88	0.5	92.17	0	3.83
	5	0.5	0	1	0	89.17	0
	6	0	0	0	1.83	0	94.5

TABLE 3. Confusion matrix after voting.

		Actual class					
		1	2	3	4	5	6
Predicted class	1	93.33	0	18.33	0	0	0
	2	0	100	0	3.33	0	1.67
	3	6.67	0	80	0	8.33	0
	4	0	0	0	96.67	0	3.33
	5	0	0	1.67	0	91.67	0
	6	0	0	0	0	0	95

Figure 5. Some of the HR images that used to evaluate the proposed method.

Comparing the diagonal values on the confusion matrices in the tables shows improvement in classification accuracy for almost all classes by voting. Considering the size of the blurring kernels according to Table 1, it is worth to note that the misclassification (non-zero off-diagonal values of the confusion matrix) is only occurred between *same size* kernels after voting. In Table 4, the list of the images with false prediction kernels is shown. More training data may be needed to achieve a higher classification accuracy.

After determining the blurring kernel for each pair of (a, b), the HR image is estimated using the LR images according to the diagram in Figure 4. For super-resolution process, we use the variational Bayesian super-resolution algorithm presented in [3].

TABLE 4. Images with false prediction kernel. Despite the error in predicting kernels, kernel sizes are predicted correctly

True kernel (size)	Predicted kernel (size)	Image #
1 (5 × 5)	3 (5 × 5)	32, 34, 35, 54
3 (5 × 5)	1 (5 × 5)	5, 10, 21, 22, 30, 39, 40, 41, 42, 43, 44
3 (5 × 5)	5 (5 × 5)	33
4 (11 × 11)	2 (11 × 11)	22, 33
5 (5 × 5)	3 (5 × 5)	5, 30, 44, 46, 48
6 (11 × 11)	2 (11 × 11)	33
6 (11 × 11)	4 (11 × 11)	44, 46

To evaluate performance of the proposed method, structural similarity index (SSIM) [13] and mean square error (MSE) between the constructed HR image and the original one are used. Table 5 shows these evaluation metric for all 60 HR images and 6 predetermined blur kernels combinations. At the bottom of this table average of the evaluation metric are shown for all images and for the images with true predicted blurring kernel. Comparing these values shows that true prediction of blurring kernel leads to more accurate SR reconstruction. In Figure 6 some of the reconstructed HR images as well as the one from the corresponding LR image are shown. As shown in this figure, given a true observation model with different blurring degradation leads to approximately same reconstructed HR image.

TABLE 5. SSIM/MSE from the experiments as well as their average

Image #	Kernel 1	Kernel 2	Kernel 3	Kernel 4	Kernel 5	Kernel 6
1	0.88/2.35E-04	0.81/2.84E-04	0.88/2.36E-04	0.76/2.90E-04	0.89/2.28E-04	0.83/2.71E-04
2	0.92/9.94E-05	0.87/1.36E-04	0.91/9.51E-05	0.85/1.33E-04	0.92/8.56E-05	0.87/1.26E-04
3	0.93/1.61E-04	0.85/5.00E-04	0.93/1.63E-04	0.85/4.36E-04	0.92/1.27E-04	0.88/3.05E-04
4	0.95/4.47E-05	0.90/6.50E-05	0.94/4.69E-05	0.89/7.14E-05	0.95/4.44E-05	0.91/5.94E-05
5	0.93/2.52E-04	0.88/3.08E-04	0.85/2.52E-04	0.88/2.98E-04	0.50/3.75E-04	0.89/2.87E-04
6	0.97/2.12E-05	0.94/3.27E-05	0.97/2.22E-05	0.94/3.70E-05	0.97/1.95E-05	0.95/2.98E-05
7	0.93/5.41E-05	0.87/7.19E-05	0.93/5.54E-05	0.85/7.74E-05	0.94/5.18E-05	0.89/6.52E-05
8	0.95/3.67E-05	0.91/5.58E-05	0.95/3.71E-05	0.89/6.48E-05	0.94/3.53E-05	0.92/4.91E-05
9	0.95/4.37E-05	0.90/6.96E-05	0.95/4.62E-05	0.89/8.14E-05	0.94/3.92E-05	0.92/5.68E-05
10	0.93/6.51E-05	0.84/9.66E-05	0.80/9.31E-05	0.81/1.08E-04	0.92/5.92E-05	0.88/8.06E-05
11	0.96/4.84E-05	0.92/6.83E-05	0.96/4.86E-05	0.90/7.07E-05	0.96/4.84E-05	0.94/6.08E-05
12	0.95/8.83E-05	0.92/1.05E-04	0.96/8.84E-05	0.92/1.06E-04	0.96/8.79E-05	0.94/9.71E-05
13	0.97/6.18E-05	0.94/6.46E-05	0.97/6.19E-05	0.94/6.54E-05	0.97/5.64E-05	0.95/6.32E-05
14	0.96/4.33E-05	0.92/6.80E-05	0.96/4.46E-05	0.90/7.89E-05	0.96/4.16E-05	0.94/5.68E-05
15	0.96/2.56E-05	0.93/3.93E-05	0.97/2.60E-05	0.92/4.49E-05	0.96/2.58E-05	0.94/3.49E-05
16	0.97/2.51E-05	0.95/3.86E-05	0.97/2.50E-05	0.95/3.92E-05	0.98/2.45E-05	0.96/3.20E-05
17	0.92/1.19E-04	0.84/1.37E-04	0.92/1.20E-04	0.80/1.43E-04	0.92/1.12E-04	0.87/1.32E-04
18	0.94/3.26E-05	0.88/5.23E-05	0.94/3.35E-05	0.87/5.48E-05	0.95/3.05E-05	0.91/4.33E-05
19	0.97/2.96E-05	0.94/4.62E-05	0.97/3.11E-05	0.94/5.22E-05	0.97/2.71E-05	0.95/3.91E-05
20	0.96/1.24E-04	0.92/1.35E-04	0.96/1.24E-04	0.91/1.37E-04	0.96/1.23E-04	0.94/1.33E-04
21	0.89/4.58E-04	0.84/5.42E-04	0.73/4.69E-04	0.85/5.42E-04	0.89/4.22E-04	0.85/5.32E-04
22	0.95/3.38E-05	0.90/5.60E-05	0.82/7.00E-05	0.51/1.68E-04	0.94/3.21E-05	0.92/4.76E-05
23	0.94/6.29E-05	0.90/1.12E-04	0.94/6.83E-05	0.88/1.45E-04	0.94/7.36E-05	0.91/8.65E-05
24	0.92/4.75E-05	0.85/7.73E-05	0.92/5.08E-05	0.83/8.77E-05	0.92/3.92E-05	0.86/7.05E-05
25	0.93/4.14E-05	0.89/6.64E-05	0.94/4.31E-05	0.88/7.76E-05	0.93/3.91E-05	0.89/6.32E-05
26	0.96/2.08E-05	0.94/4.07E-05	0.96/2.11E-05	0.94/3.91E-05	0.97/1.86E-05	0.95/3.29E-05
27	0.95/3.43E-05	0.90/5.18E-05	0.95/3.55E-05	0.88/5.89E-05	0.95/3.29E-05	0.93/4.30E-05
28	0.94/3.48E-05	0.89/6.54E-05	0.95/3.73E-05	0.86/7.78E-05	0.94/2.97E-05	0.92/4.56E-05
29	0.96/4.29E-05	0.93/6.93E-05	0.96/4.36E-05	0.93/7.66E-05	0.95/4.25E-05	0.94/5.94E-05
30	0.95/2.44E-05	0.89/3.79E-05	0.88/4.11E-05	0.86/4.35E-05	0.39/1.75E-04	0.92/3.08E-05
31	0.94/5.85E-05	0.85/1.19E-04	0.93/6.04E-05	0.81/1.21E-04	0.94/5.37E-05	0.90/8.84E-05
32	0.78/1.51E-04	0.89/1.27E-04	0.94/6.95E-05	0.87/1.44E-04	0.94/7.46E-05	0.91/1.10E-04
33	0.97/2.33E-05	0.95/3.24E-05	0.87/1.02E-04	0.56/1.58E-04	0.97/2.40E-05	0.25/3.52E-04
34	0.80/1.51E-04	0.86/1.24E-04	0.94/7.79E-05	0.80/1.45E-04	0.95/6.73E-05	0.90/1.03E-04
35	0.87/1.13E-04	0.93/1.26E-04	0.96/6.08E-05	0.92/1.26E-04	0.95/5.53E-05	0.94/8.74E-05
36	0.87/1.60E-04	0.69/2.03E-04	0.85/1.60E-04	0.62/2.10E-04	0.91/1.36E-04	0.81/1.78E-04

37	0.94/6.55E-05	0.88/1.29E-04	0.94/6.64E-05	0.84/1.43E-04	0.95/5.72E-05	0.90/1.15E-04
38	0.87/6.77E-04	0.80/8.16E-04	0.87/6.78E-04	0.77/8.05E-04	0.88/6.34E-04	0.84/7.68E-04
39	0.96/1.48E-04	0.93/1.62E-04	0.86/1.63E-04	0.93/1.65E-04	0.96/1.48E-04	0.94/1.59E-04
40	0.97/2.69E-05	0.94/3.79E-05	0.93/3.39E-05	0.93/3.94E-05	0.97/2.70E-05	0.95/3.38E-05
41	0.97/9.77E-05	0.95/1.54E-04	0.89/1.88E-04	0.94/1.64E-04	0.97/1.02E-04	0.96/1.30E-04
42	0.93/1.86E-04	0.88/2.00E-04	0.86/1.97E-04	0.86/2.03E-04	0.93/1.79E-04	0.90/1.98E-04
43	0.95/3.57E-04	0.92/4.15E-04	0.87/3.92E-04	0.91/4.24E-04	0.95/3.56E-04	0.93/4.06E-04
44	0.97/1.12E-04	0.95/1.79E-04	0.91/1.14E-04	0.95/1.72E-04	0.51/2.53E-04	0.42/3.28E-04
45	0.92/1.77E-04	0.86/1.90E-04	0.91/1.71E-04	0.85/1.93E-04	0.90/1.78E-04	0.88/1.89E-04
46	0.95/4.79E-05	0.90/7.64E-05	0.95/5.02E-05	0.88/9.01E-05	0.50/2.98E-04	0.43/3.03E-04
47	0.96/4.47E-05	0.90/1.52E-04	0.96/4.65E-05	0.90/1.53E-04	0.95/4.20E-05	0.92/1.26E-04
48	0.96/4.81E-04	0.90/8.83E-04	0.96/4.82E-04	0.90/8.30E-04	0.50/8.75E-04	0.93/7.25E-04
49	0.96/2.16E-04	0.92/2.89E-04	0.96/2.16E-04	0.92/2.91E-04	0.96/1.93E-04	0.93/2.53E-04
50	0.90/1.52E-04	0.78/1.96E-04	0.89/1.54E-04	0.71/1.99E-04	0.92/1.39E-04	0.84/1.80E-04
51	0.95/3.08E-04	0.91/3.52E-04	0.95/2.98E-04	0.91/3.53E-04	0.94/2.88E-04	0.93/3.40E-04
52	0.93/1.13E-04	0.85/2.84E-04	0.93/1.14E-04	0.81/2.87E-04	0.93/9.32E-05	0.89/2.18E-04
53	0.95/1.07E-04	0.90/1.32E-04	0.95/1.07E-04	0.85/1.45E-04	0.95/8.81E-05	0.93/1.19E-04
54	0.85/8.06E-05	0.91/1.28E-04	0.96/4.79E-05	0.91/1.19E-04	0.96/4.38E-05	0.93/8.66E-05
55	0.89/5.00E-05	0.80/6.97E-05	0.88/5.31E-05	0.77/7.57E-05	0.92/4.12E-05	0.83/6.19E-05
56	0.93/1.29E-04	0.88/1.41E-04	0.93/1.25E-04	0.86/1.48E-04	0.92/1.25E-04	0.90/1.40E-04
57	0.96/1.47E-04	0.93/2.23E-04	0.96/1.47E-04	0.92/2.18E-04	0.96/1.47E-04	0.95/1.86E-04
58	0.95/6.36E-05	0.91/1.01E-04	0.95/6.73E-05	0.90/1.24E-04	0.95/5.97E-05	0.93/8.28E-05
59	0.91/1.46E-04	0.87/1.73E-04	0.90/1.46E-04	0.86/1.74E-04	0.91/1.41E-04	0.87/1.68E-04
60	0.96/7.01E-05	0.91/1.77E-04	0.96/7.20E-05	0.91/1.60E-04	0.95/6.92E-05	0.93/1.09E-04
mean (all)	0.93/1.18E-04	0.89/1.65E-04	0.92/1.20E-04	0.86/**1.71E-04**	0.90/1.26E-04	0.88/1.56E-04
mean (truly detected)	**0.94**/**1.17E-04**	0.89/1.65E-04	**0.94**/**1.06E-04**	**0.87**/1.72E-04	**0.94**/**1.01E-04**	**0.91**/**1.47E-04**

(a) Image # 3

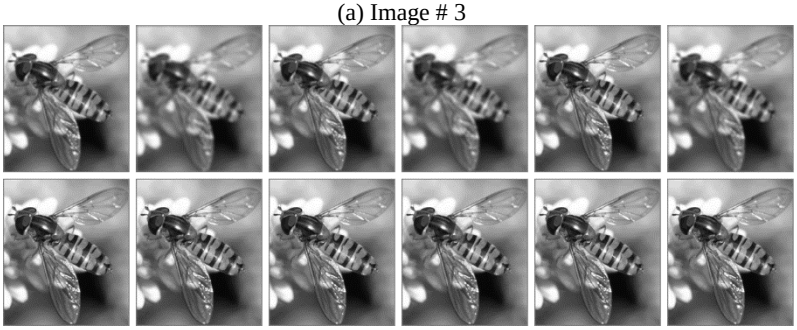

(b) Image # 19

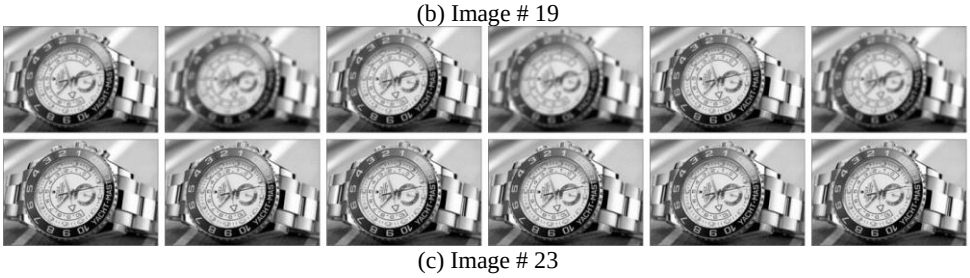

(c) Image # 23

(d) Image # 35

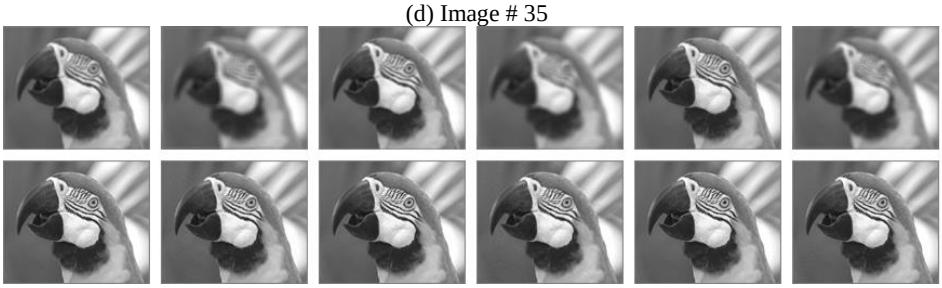

(e) Image # 58

Figure 6. Results of the proposed method. *Up row*: one of the LR images. *Bottom row*: reconstructed HR image. Columns 1 through 6 correspond to kernels 1 through 6, respectively

(a) Image # 22, misclassified kernel: 3, 4

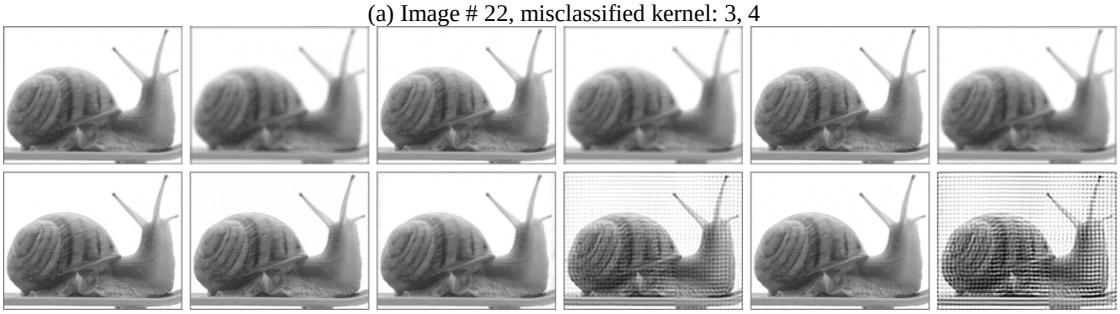

(b) Image # 33, misclassified kernel: 3, 4, 6

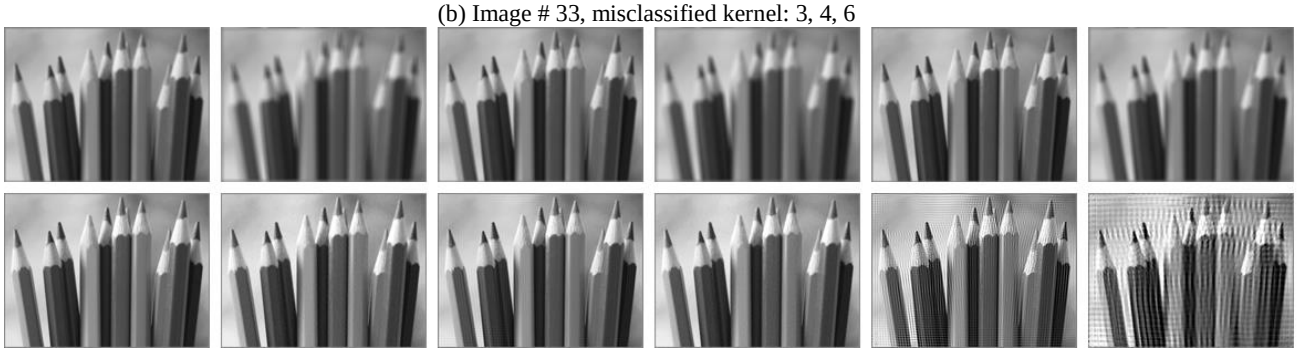

(c) Image # 44, misclassified kernel: 5, 6

Figure 7. Some of images with a false predicted kernel. *Up row*: one of the LR images. *Bottom row*: reconstructed HR image. Columns 1 through 6 correspond to kernels 1 through 6 respectively

Investigating the evaluation metric on the images with a false prediction kernel (Table 4) in Table 5 shows that truly determining the blurring kernel in constructing HR images is vital.

Figure 7 shows some of these reconstructed HR images with a false predicted kernel, as well as one corresponding LR image. As shown in this figure, the most artifact is produced in reconstructing image # 33 (Snail) and image # 44 (colored pencils) both for kernel 6 (the left image in the second row of Figure 7b and 7c). To justify the need of the true kernel in SR, the reconstruction of HR image, given *true* kernel, for these two samples is depicted in Figure 8.

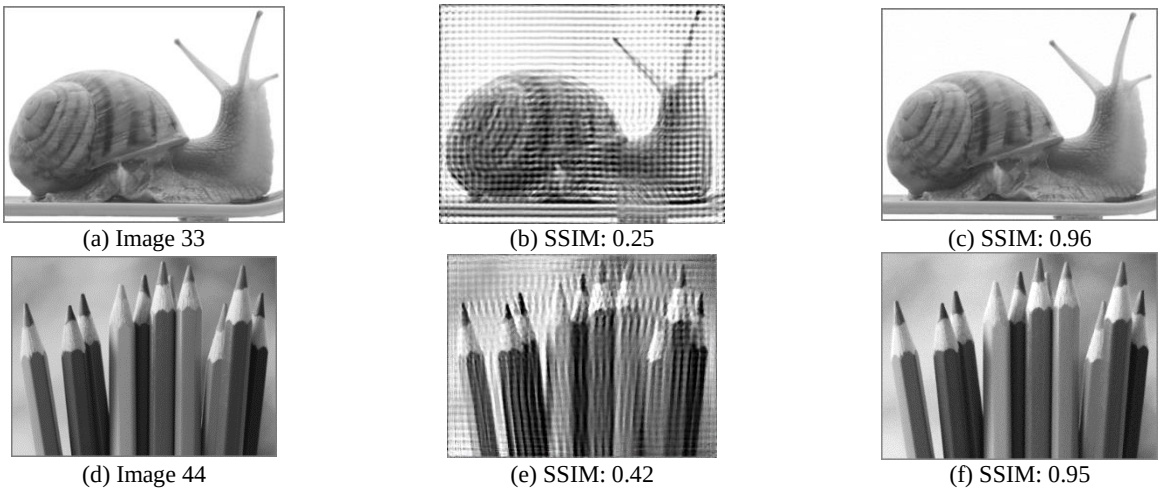

(a) Image 33 (b) SSIM: 0.25 (c) SSIM: 0.96

(d) Image 44 (e) SSIM: 0.42 (f) SSIM: 0.95

Figure 8. Importance of using true kernel in SR. *a, d)* Original image, *b, e)* Reconstruction using wrong kernel, *c, f)* Reconstruction using true kernel

5. CONCLUSION

To estimate high resolution (HR) image accurately using super-resolution (SR), the details of the acquisition process are required. In SR such knowledge is modeled as observation model. This model is constructed by warping, blurring, down-sampling operators as well as the noise. In this paper, a method to predict the blurring operator in the simulated framework is proposed. Specifically, we use neural network to predict the class of the HR image blur kernel given the blur kernel of the low resolution (LR) images.

It is worth noting that the efficiency of the blur kernel estimation algorithm is very important, as error in blur kernel estimation leads to false prediction class of HR blurring kernel.

As a future work, estimation of the HR blur kernel from the estimated LR blur kernel in a regression approach can be investigated. The kernel estimated using such an approach can be used to apply the super resolution technique to LR images taken by a camera.

6. REFERENCES

1. Katsaggelos, A.K., Molina, R. and Mateos, J., "Super resolution of images and video", ***Synthesis Lectures on Image, Video, and Multimedia Processing***, Vol. 1, No. 1, (2007), 1-134.
2. Farsiu, S., Robinson, M.D., Elad, M. and Milanfar, P., "Fast and robust multiframe super resolution", ***IEEE Transactions on Image Processing***, Vol. 13, No. 10, (2004), 1327-1344.
3. Babacan, S.D., Molina, R. and Katsaggelos, A.K., "Variational bayesian super resolution", ***IEEE Transactions on Image Processing***, Vol. 20, No. 4, (2011), 984-999.
4. Tsai, R., "Multiframe image restoration and registration", ***Advance Computer Visual and Image Processing***, Vol. 1, (1984), 317-339.
5. Tipping, M.E. and Bishop, C.M., "Bayesian image super-resolution", in Advances in neural information processing systems. (2003), 1303-1310.
6. Nguyen, N., Milanfar, P. and Golub, G., "Efficient generalized cross-validation with applications to parametric image restoration and resolution enhancement", ***IEEE Transactions on Image Processing***, Vol. 10, No. 9, (2001), 1299-1308.
7. Aly, H.A. and Dubois, E., "Specification of the observation model for regularized image up-sampling", ***IEEE Transactions on Image Processing***, Vol. 14, No. 5, (2005), 567-576.
8. Sroubek, F., Cristóbal, G. and Flusser, J., "A unified approach to superresolution and multichannel blind deconvolution", ***IEEE Transactions on Image Processing***, Vol. 16, No. 9, (2007), 2322-2332.
9. Laghrib, A., Ezzaki, M., El Rhabi, M., Hakim, A., Monasse, P. and Raghay, S., "Simultaneous deconvolution and denoising using a second order variational approach applied to image super resolution", ***Computer Vision and Image Understanding***, (2017).
10. Javaran, T.A., Hassanpour, H. and Abolghasemi, V., "Non-blind image deconvolution using a regularization based on re-blurring

process", ***Computer Vision and Image Understanding***, Vol. 154, (2017), 16-34.

11. Nair, V. and Hinton, G.E., "Rectified linear units improve restricted boltzmann machines", in Proceedings of the 27th international conference on machine learning (ICML-10). (2010), 807-814.
12. Russakovsky, O., Deng, J., Su, H., Krause, J., Satheesh, S., Ma, S., Huang, Z., Karpathy, A., Khosla, A. and Bernstein, M., "Imagenet large scale visual recognition challenge", ***International Journal of Computer Vision***, Vol. 115, No. 3, (2015), 211-252.
13. Wang, Z., Bovik, A.C., Sheikh, H.R. and Simoncelli, E.P., "Image quality assessment: From error visibility to structural similarity", ***IEEE Transactions on Image Processing***, Vol. 13, No. 4, (2004), 600-612.

Improving Super-resolution Techniques via Employing Blurriness Information of the Image

S. J. Seyyedyazdi, H. Hassanpour

Faculty of Computer Engineering and IT, Shahrood University of Technology, Shahrood, Iran

P A P E R I N F O

Paper history:
Received 05 October 2017
Received in revised form 01 November 2017
Accepted 30 November 2017

Keywords:
Super-resolution
Blur Kernel
Blur Kernel Estimation
Neural Network

چکیده

ابرتفکیک‌پذیری فنی است که با استفاده از آن می‌توان با ترکیب چند تصویر با دقت کم از یک صحنه، تصویری با دقت بالا ایجاد کرد. یکی از مشکلاتی که کارایی این تکنیک را کم می‌کند، تاری در تصاویر ورودی است. در بسیاری از کارهای انجام شده در زمینه‌ی ابرتفکیک‌پذیری تاری تصاویر کم دقت ناشی از خاصیت انتگرال‌گیری حس‌گر تصویر در دستگاه تصویربرداری فرض شده است؛ در حالی که در عمل عوامل دیگری نیز وجود دارد که موجب تاری تصویر کم دقت می‌شوند. از جمله‌ی این عوامل می‌توان به پراش نور، حرکت جسم یا دستگاه تصویربرداری یا هر دو، تاری ناشی از اغتشاش هوا و تاری ناشی از عدم تمرکز عدسی دوربین اشاره کرد. برای اعمال دقیق ابرتفکیک‌پذیری نیاز است که مدل تخریب اعمال شده بر روی تصویر دقت بالا (ایده‌آل) در فرآیند تولید تصویر کم دقت مشخص باشد. در این مقاله هدف ما بررسی تاری در تصاویر کم دقت برای یافتن هسته‌ی تاری اعمال شده به تصویر دقت بالاست. از این رو یک آزمایش شبیه‌سازی ترتیب داده‌ایم که در آن هسته‌های تاری، محدود به چند هسته‌ی از پیش تعیین شده هستند. در این آزمایش تاری تصاویر کم دقت نامعلوم فرض شده است و به‌وسیله‌ی یکی از روش‌های تخمین تاری به دست می‌آیند. آنگاه، هسته‌های تاری برآورد شده مربوط به تصاویر کم دقت به یک شبکه‌ی عصبی مصنوعی داده می‌شوند تا هسته‌های تاری مربوط به تصاویر دقت بالا را تعیین کند. نتایج آزمایش‌ها نشان می‌دهد که استفاده از هسته‌های تاری تعیین شده توسط شبکه‌ی عصبی، کیفیت تصویر دقت بالای خروجی را افزایش می‌دهد.

***doi**: 10.5829/ije.2018.31.02b.07*